Winter 11-28-2018

Near-Infrared Photoluminescence and Electrochemiluminescence from an Exceptionally Simple Boron Difluoride Formazanate Dye

Ryan R. Maar

Ruizhong Zhang

David G. Stephens

Zhifeng Ding

Joe Gilroy
jgilroy5@uwo.ca

Near-Infrared Photoluminescence and Electrochemiluminescence from an Exceptionally Simple Boron Difluoride Formazanate Dye

Ryan R. Maar†, Ruizhong Zhang†, David G. Stephens, Zhifeng Ding* and Joe B. Gilroy*

Abstract: Electrochemiluminescence involves the generation of light via electrochemical reactions and has recently shown utility for single-cell imaging. To further develop this novel imaging platform, it is necessary to produce readily available dyes that photoluminesce and electrochemiluminesce in the near-infrared region to limit absorption by biological tissue. To address this need, we prepared a boron difluoride formazanate dye that exhibits near-infrared photoluminescence and electrochemiluminescence in two straightforward synthetic steps. Examination of its solid-state structure suggests that the *N*-aryl substituents have significant quinoidal character, which narrows the S_1-S_0 energy gap and leads to near-infrared absorption and photoluminescence. Electrochemical properties were probed using cyclic voltammetry and revealed four electrochemically reversible waves. Electrochemiluminescence properties were examined in the presence of tri-*n*-propylamine, leading to maximum intensity at 910 nm, at least 85 nm (1132 cm^{-1}) red-shifted compared to all other organic dyes. This work sets the stage for the development of future generations of dyes for emerging applications, including single-cell imaging, that require near-infrared photoluminescence and electrochemiluminescence.

Materials capable of near-infrared (NIR) light absorption and photoluminescence (PL) are of considerable interest to the fields of materials science[1] and biomedical imaging.[2] For the latter, NIR light is minimally absorbed by the skin and other biological tissues, which enhances light penetration[3] and minimizes autofluorescence from biological molecules (*e.g.*, hemoglobin).[4] As a result, NIR dyes have enhanced utility for photodynamic[5] and photothermal therapy,[6] and for *in vivo* cellular imaging.[2b, 7] Recently, electrochemiluminescence or electrogenerated chemiluminescence (ECL)[8] microscopy has also been utilized for single-cell imaging.[9]

For ECL to occur, highly reactive radical species must be electrochemically generated in the vicinity of the working electrode. These intermediates then participate in an electron-transfer reaction to generate an excited state, which returns to the ground state via radiative relaxation.[8a, 8b] ECL spectroscopy is an extremely sensitive analytical technique capable of picomolar to femtomolar (*i.e.,* 10^{-12}–10^{-15} M) detection levels.[10] In addition, it benefits from impressive signal-to-noise ratios, excellent temporal and spatial control, and low-cost.[11] As a result of these advantages, the development of dyes capable of NIR ECL is of paramount importance for future application in biological sensing and imaging. While NIR ECL systems based on inorganic nanomaterials[12] (*e.g.*, $Au_{25}(SC_2H_4Ph)_{18}^-$,[13] $Au_{38}(SC_2H_4Ph)_{24}$,[14] and $CuInS_2$[15]) have been reported, only a few organic dyes capable of NIR ECL are known.[16] For example, Bard and co-workers explored the NIR ECL of a heptamethine cyanine dye **1** and tricarbocyanine dye **2**. Both molecules require extended π-systems to achieve efficient NIR absorption and luminescence.[17] Dyes **1** and **2** have wavelengths of maximum absorption (λ_{max}) and PL (λ_{PL}) in the NIR region and in the presence of tri-*n*-propylamine (TPrA), exhibited peak ECL intensity at wavelengths (λ_{ECL}) of 805 nm and 825 nm, respectively. Despite an approximate two-fold increase in molecular weight from dye **1** (570.91 g mol^{-1}) to dye **2** (1008.35 g mol^{-1}) the λ_{ECL} was only shifted by 20 nm. In order to red-shift the maximum further into the NIR region, a larger π-system would likely need to be realized. This represents a major hurdle in the development of organic dyes which exhibit NIR ECL, as routes to generate extended/fused π-systems can be synthetically demanding. Herein, we describe a low molecular weight boron difluoride (BF_2) formazanate dye **3** capable of NIR PL and ECL. Its straightforward, two-step synthesis in combination with its exceptionally simple structure represent a significant advantage in the development of readily accessible dyes for NIR PL and ECL applications.

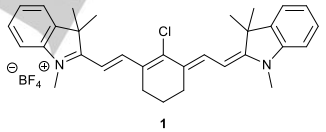

MW = 570.91 g mol^{-1}
λ_{abs} = 774 nm
λ_{PL} = 800 nm
λ_{ECL} = 805 nm

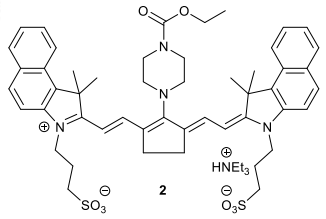

MW = 1008.35 g mol^{-1}
λ_{abs} = 738 nm
λ_{PL} = 820 nm
λ_{ECL} = 825 nm

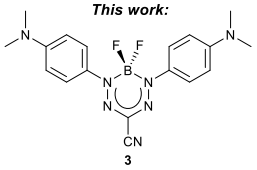

MW = 383.21 g mol^{-1}
λ_{abs} = 728 nm
λ_{PL} = 888 nm
λ_{ECL} = 910 nm

Formazan **4** was prepared by adapting a published procedure.[18] Its identity and purity were confirmed using NMR spectroscopy, FT-IR spectroscopy and UV-vis absorption spectroscopy, and mass spectrometry (Figures S1–S3). Formazan **4** gave rise to a singlet at 12.05 ppm in its ^{1}H NMR spectrum as well as a low-energy λ_{max} of 534 nm that are comparable to structurally related 3-cyanoformazans.[18,19] BF_2 formazanate **3** was prepared by heating formazan **4** at 80 °C in toluene with excess NEt_3 and BF_3•OEt_2 (Scheme 1). Purification via column chromatography afforded the dye in 60% yield, which was characterized using NMR spectroscopy, FT-IR spectroscopy, and mass spectrometry (Figures S4 and S5). This transformation was accompanied by a colour change from purple to blue-green, as well as a loss of the diagnostic NH

[a] R.R. Maar, Dr. R. Zhang, D. Stephens, Prof. Dr. Z. Ding, Prof. Dr. J. B. Gilroy
Department of Chemistry and The Centre for Advanced Materials and Biomaterials Research
The University of Western Ontario
1151 Richmond Street North, London, Ontario N6A 5B7 (Canada)
E-mail: zfding@uwo.ca, joe.gilroy@uwo.ca

† Contributed equally to this work

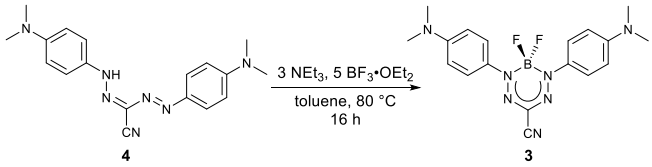

Scheme 1. Synthesis of BF_2 formazanate **3**.

resonance associated with formazan **4** and the appearance of a triplet at –0.4 ppm in the ^{11}B NMR spectrum and a quartet at –137.4 ppm in the ^{19}F NMR spectrum.

Single crystals suitable for X-ray diffraction were grown by vapor diffusion of hexanes into a saturated CH_2Cl_2 solution containing **3** (Tables S1 and S2). The asymmetric unit of dye **3** contained two unique conformers (Figures 1 and S6). Further analysis revealed that the boron atoms adopt a slightly distorted tetrahedral geometry and the average angles between the plane defined by the *N*-aryl substituents and the four nitrogen atoms of the formazanate backbone (N_4: N1, N2, N3, N4) were 18.63° (conformer A) and 27.44° (conformer B). In addition, the boron atoms are displaced from the N_4 plane by 0.136 Å and 0.321 Å for conformers A and B, respectively. The N-C [1.3315(16)–1.3434(15) Å] and N-N [1.3113(13)–1.3143(13) Å] bond lengths of the formazanate ligand backbone are between what would normally be expected for single and double bonds of the same atoms[20] indicating that the π-system is highly delocalized. The latter are elongated compared to typical N-N bond lengths reported for related BF_2 formazanates.[19, 21] Examination of the average N-C [N6-C6: 1.3647(16), N7-C12: 1.3629(16)] bond lengths between the dimethylamino nitrogen atom and the adjacent carbon atom are indicative of a bond order of *ca.* 1.5. Similarly, the average N1-C3 [1.4110(16)] and N3-C9 [1.4110(16)] bond lengths also indicate a bond order of *ca.* 1.5 and are substantially shorter than those observed for related BF_2 formazanates.[19] These metrics suggest that the *N*-aryl substituents of dye **3** possess significant quinoidal character, a trait that has not previously been observed for this family of dyes. Given that the frontier molecular orbital isosurfaces calculated for related BF_2 formazanates include density at both the formazanate backbone and the *N*-aryl substituents,[19] this quinoidal character is expected to dramatically enhance electronic delocalization and shift absorption, PL, and ECL spectra to lower energies.

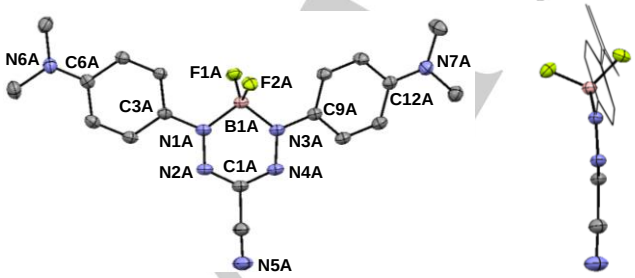

Figure 1. Top and side views of one conformer of BF_2 formazanate **3** found within the unit cell of the determined solid-state structure. Anisotropic displacement ellipsoids are shown at the 50% probability level and hydrogen atoms have been omitted for clarity. *N*-aryl substituents (side view) have been displayed as wireframe for clarity.

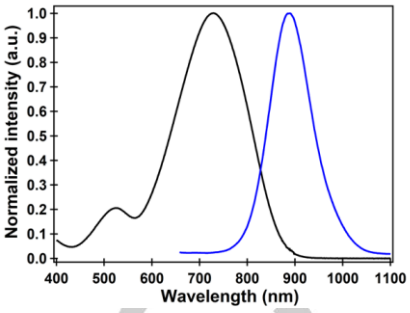

Figure 2. Normalized UV-vis absorption (black line) and PL (blue line) spectra recorded for a 6 μM dry, degassed CH_3CN solution of dye **3**.

The UV-vis absorption and PL spectra of dye **3** were recorded in toluene, CH_2Cl_2, THF, and CH_3CN (Figures 2 and S7, Table S3) and are consistent with the enhanced delocalization evident in the solid-state structure. Dye **3** is strongly absorbing (ε = 38600–47800 M^{-1} cm^{-1}) in the NIR spectral region and the λ_{max} values observed were relatively insensitive to the solvent polarity (toluene: λ_{max} = 728 nm, CH_2Cl_2: λ_{max} = 733 nm, THF: λ_{max} = 731 nm, CH_3CN: λ_{max} = 728 nm). Previous work on related BF_2 formazanates showed that the HOMO and LUMO are the dominant orbital pair involved in the lowest energy excitation, which has significant π→π* character.[22] The PL spectra showed that the solvent polarity has a larger effect on the λ_{PL} and ranges from 834 nm to 888 nm (Figures 2 and S7, Table S3). The appreciable PL quantum yields (Φ_{PL}, Equation S1 in the Supporting Information) determined for BF_2 formazanate **3** varied minimally in four different solvents [Φ_{PL}: 8% (toluene), 4% (CH_2Cl_2), 5% (THF), 3% (CH_3CN)]. It should be noted that dyes which exhibit NIR PL often give rise to lower Φ_{PL} values compared to systems that luminesce within the visible region as the former have smaller S_1-S_0 energy gaps, which can result in an increased probability of non-radiative relaxation events, as described by the energy gap law.[23] This is particularly important given that dye **3** exhibits PL (*ca.* 750–1050 nm) in both the NIR 1 and NIR 2 regions. Dye **3** also exhibits relatively large Stokes shifts (ν_{ST}) ranging from 106 to 160 nm (1746–2475 cm^{-1}) depending on the solvent (Table S3).

A cyclic voltammogram (CV) was collected for dye **3** at a scan rate of 0.10 V s^{-1} in CH_3CN containing [nBu$_4$N][PF_6] (Figure 3A and Table S3). Upon scanning to negative potentials, two reversible one-electron waves were evident and correspond to the reduction of BF_2 formazanate **3** to its ligand-centred radical anion (**3**$^{\bullet-}$, E°_{red1} = –1.02 V relative to the ferrocene/ferrocenium redox couple) and dianion (**3**$^{2-}$, E°_{red2} = –2.05 V). Upon scanning to positive potentials, two reversible one-electron oxidations were also observed and assigned to the formation of ligand-centred radical cation (**3**$^{\bullet+}$, E°_{ox1} = 0.27 V) and dication (**3**$^{2+}$, E°_{ox2} = 0.56 V), respectively. The unique electrochemical features of BF_2 formazanate **3** in combination with its NIR PL prompted us to investigate its potential NIR ECL.

The ECL of BF_2 formazanate **3** was examined in the absence and presence of TPrA as a coreactant. In the absence of a coreactant, ECL was not detected between –2.35 V and 0.85 V (Figure 3A). This is likely a result of the insufficient lifetimes of

the electrogenerated species in the vicinity of the working electrode that would be required for ECL.

The introduction of a coreactant often results in enhanced ECL, as the coreactant and analyte-based radicals required to produce the excited state exist at similar potentials.[8a, 8b, 11a] Figure 3B displays the CV along with the ECL-voltage curve for **3** in the presence of TPrA (15 mM). The TPrA• radical, generated upon oxidation of TPrA and subsequent loss of a proton, has emerged as a useful coreactant for the enhancement of ECL and is a potent reductant.[24] The onset of ECL for dye **3** was observed at 0.35 V and the ECL-voltage curve had a maximum intensity at a potential of 0.54 V, where $\mathbf{3}^{\bullet+}$ and TPrA• co-exist in appreciable quantities (Equations 1 and 2).[11a, 24] An excited state $\mathbf{3}^{*}$ is generated when $\mathbf{3}^{\bullet+}$ and TPrA• react (Equation 3), leading to ECL when the excited state relaxes to the ground state (Equation 4). On scanning to more positive potentials, a second ECL maximum was observed at a potential of 0.95 V. At this potential, the solution likely contains

$$\mathbf{3} \xrightarrow{-e^-} \mathbf{3}^{\bullet+} \xrightarrow{-e^-} \mathbf{3}^{2+} \quad (1)$$

$$\text{TPrA} \xrightarrow{-e^-} \text{TPrA}^{\bullet+} \xrightarrow{-H^+} \text{TPrA}\bullet \quad (2)$$

$$\mathbf{3}^{\bullet+} + \text{TPrA}\bullet \longrightarrow \mathbf{3}^{*} + Pr_2N^+{=}CHCH_2CH_3 \quad (3)$$

$$\mathbf{3}^{*} \longrightarrow \mathbf{3} + h\nu \quad (4)$$

$$\mathbf{3} + \mathbf{3}^{2+} \longrightarrow 2\,\mathbf{3}^{\bullet+} \quad (5)$$

significant quantities of electrogenerated $\mathbf{3}^{2+}$ and TPrA•. We postulate that $\mathbf{3}^{2+}$ and **3** can undergo a comproportionation reaction based on previous computational studies (Equation 5),[25] and that lower ECL intensity in this region likely relates to the two-step process required to generate $\mathbf{3}^{\bullet+}$ in the vicinity of the working electrode at these higher potentials.

ECL efficiencies (Φ_{ECL}) were calculated relative to the $[Ru(bpy)_3][PF_6]_2$/TPrA coreactant system using the ratio of ECL intensity obtained from the accumulated ECL spectra and the total charge from the corresponding CV (Equation S2 in Supporting Information). To obtain the optimal experimental results, we explored the scan rate dependence of a CH_3CN solution containing 0.05 mM **3**, 15 mM TPrA, and 0.1 M $[n\text{Bu}_4\text{N}][PF_6]$ as supporting electrolyte by scanning eight consecutive cycles from –0.35 to 0.95 V (Figure S8, Table S4). These experiments revealed a maximum Φ_{ECL} of 17.5% at a scan rate of 0.20 V s^{-1}. Despite the red-shifted λ_{ECL} that should lead to diminished Φ_{ECL} according to the energy gap law,[23] the observed efficiency of **3**/TPrA was similar to **1**/TPrA (Φ_{ECL} = 21%)[16a] and **2**/TPrA (Φ_{ECL} = 17%)[16b], which possess significantly larger π-systems and more complex structures. At reduced scan rates, the **3**/TPrA system exhibited lower Φ_{ECL} values likely due to decreased concentrations of $\mathbf{3}^{\bullet+}$ as a result of decomposition that is enhanced on these longer timescales. Furthermore, we explored the effect of increasing the concentration of TPrA from 15 to 30 mM in 5 mM increments (Figure S9, Table S5). Increasing the concentration of TPrA led to higher ECL intensities, but also higher electrochemical currents in the CVs. Ultimately, lower Φ_{ECL} values were obtained as the concentration of TPrA increased.

Spooling ECL spectroscopy allowed for the evolution and devolution of ECL intensity to be monitored in real time (Figure 3). Spooling ECL experiments were conducted at various scan rates and using different concentrations of TPrA (Figures S10–S15). Figures 3C and 3G show the spooling ECL spectra and the corresponding CV recorded at a scan rate of 0.0125 V s^{-1} in the presence of 15 mM TPrA. The ECL onset potential was found at 0.40 V (t = 15 s) and reached its maximum intensity at 0.55 V (t = 18 s), in close agreement with the ECL-voltage data shown in Figure 3B. The maximum ECL intensity remained at 910 nm throughout the experiment demonstrated by the evolution and devolution ECL spectra (Figures 3D and 3E). This finding indicates that a single excited state is implicated in the ECL process. The ECL accumulated spectrum obtained over the course of eight consecutive scan cycles between –0.35 V and 0.95 V had a maximum intensity at 910 nm (Figure 3F). The 22 nm difference between the λ_{ECL} (910 nm) and λ_{PL} (888 nm) maxima is likely a result of the inner filter effect caused by self-absorption (Figures 2 and S7).[26] However, we cannot rule out excimer formation[27] as BF_2 complexes of formazanate ligands have been shown to aggregate via π-type interactions.[28] The λ_{ECL} observed during these studies is at least

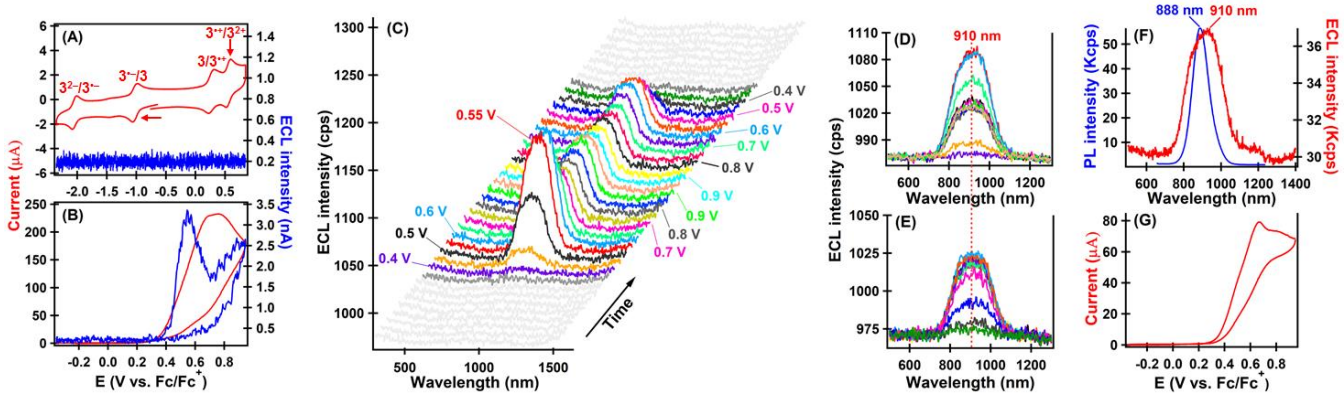

Figure 3. (A) CV (red line) and ECL-voltage curve (blue line) of a 0.05 mM CH_3CN solution of **3** containing 0.1 M $[n\text{Bu}_4\text{N}][PF_6]$ as supporting electrolyte recorded at a scan rate of 0.10 V s^{-1}. The arrow indicates the scan direction. (B) CV (red line) and ECL-voltage curve (blue line) of a 0.05 mM CH_3CN solution of **3**, 15 mM TPrA, and 0.1 M $[n\text{Bu}_4\text{N}][PF_6]$ as supporting electrolyte recorded at a scan rate of 0.20 V s^{-1}. (C) Spooling ECL spectra, (D) Evolution, (E) Devolution spectra collected for a CH_3CN solution containing 0.05 mM of dye **3**, 15 mM TPrA, and 0.1 M $[n\text{Bu}_4\text{N}][PF_6]$ as supporting electrolyte acquired by reversibly scanning between –0.35 and 0.95 V at a scan rate of 0.0125 V s^{-1} and a time interval of 4 s for each spectrum. The potential window is shown from –0.10 V to 0.95 V for clarity. (F) PL spectrum of dye **3** (blue line) and accumulated ECL spectrum of dye **3**/TPrA (red line) in CH_3CN. The accumulated spectrum was recorded at a scan rate of 0.02 V s^{-1}. (G) CV of dye **3**/TPrA recorded at 0.0125 V s^{-1}.

85 nm (1132 cm^{-1}) red-shifted compared to all other ECL organic dyes reported to date.

In conclusion, we report a BF_2 formazanate dye with a remarkably simple structure, synthesized via a straightforward two-step procedure from commercially available starting materials and capable of NIR PL and ECL. Analysis of the solid-state structure of dye **3** revealed that the *N*-aryl substituents possess significant quinoidal character, leading to enhanced electronic delocalization over the π-system that includes both the formazanate backbone and the *N*-aryl substituents. This delocalization results in a drastic red-shift in both the absorption, PL, and ECL maxima compared to related BF_2 formazanates without the need for elaborate structure alteration. The electrochemical properties of our dye were probed using cyclic voltammetry and these studies revealed two reversible reductions and two reversible oxidations within the electrochemical solvent window afforded by CH_3CN. The unique PL and electrochemical characteristics observed prompted us to investigate the ECL properties of dye **3**. In the absence of a coreactant, no ECL was observed. However, ECL was induced upon the addition of tri-*n*-propylamine and reached a maximum intensity at 0.54 V relative to the ferrocene/ferrocenium redox couple. The wavelength of maximum ECL intensity was centred at 910 nm with an efficiency of 17.5% relative to the benchmark $[Ru(bpy)_3][PF_6]_2$/TPrA system. Based on the simplicity of this dye and its unique properties, we envision that this study will inspire the development of future generations of organic dyes required for emerging applications involving NIR photoluminescent and electrochemiluminescent materials. Our future work will focus on compound **3**, its protonated/methylated analogues, and structurally related compounds in order to develop the chemistry of this family of near-IR dyes in a variety of different solvents and biologically-relevant media.

Acknowledgements

This work was supported by the Natural Sciences and Engineering Research Council (NSERC) of Canada (Z.D.: DG RGPIN-2018-04240, J.B.G.: DG RGPIN-2013-435675, R.R.M.: CGS-D Scholarship, and D.G.S.: USRA Scholarship), the Ontario Ministry of Research and Innovation (J.B.G.: ERA, ER-14-10-147), and the Canadian Foundation for Innovation (J.B.G.: JELF, 33977).

Keywords: NIR electrochemiluminescence • NIR photoluminescence • Organic dyes • Electrochemistry • Formazanate ligands

[1] a) G. Qian, Z. Y. Wang, *Chem. Asian J.* **2010**, *5*, 1006–1029; b) H. Xiang, J. Cheng, X. Ma, X. Zhou, J. J. Chruma, *Chem. Soc. Rev.* **2013**, *42*, 6128–6185; c) X. Liu, Y. Lin, Y. Liao, J. Wu, Y. Zheng, *J. Mater. Chem. C* **2018**, *6*, 3499–3513.

[2] a) L. Yuan, W. Lin, K. Zheng, L. He, W. Huang, *Chem. Soc. Rev.* **2013**, *42*, 622–661; b) Z. Guo, S. Park, J. Yoon, I. Shin, *Chem. Soc. Rev.* **2014**, *43*, 16–29; c) G. Hong, A. L. Antaris, H. Dai, *Nat. Biomed. Eng.* **2017**, *1*, 0010.

[3] R. Weissleder, *Nat. Biotechnol.* **2001**, *19*, 316–317.

[4] J. V. Frangioni, *Curr. Opin. Chem. Biol.* **2003**, *7*, 626–634.

[5] a) D. E. J. G. J. Dolmans, D. Fukumura, R. K. Jain, *Nat. Rev. Cancer* **2003**, *3*, 380–387; b) A. Kamkaew, S. H. Lim, H. B. Lee, L. V. Kiew, L. Y. Chung, K. Burgess, *Chem. Soc. Rev.* **2013**, *42*, 77–88; c) Z. Zhou, J. Song, L. Nie, X. Chen, *Chem. Soc. Rev.* **2016**, *45*, 6597–6626; d) A. P. Thomas, L. Palanikumar, M. T. Jeena, K. Kim, J.-H. Ryu, *Chem. Sci.* **2017**, *8*, 8351–8356; e) L. Jiao, F. Song, J. Cui, X. Peng, *Chem. Commun.* **2018**, *54*, 9198–9201.

[6] a) H. S. Jung, P. Verwilst, A. Sharma, J. Shin, J. L. Sessler, J. S. Kim, *Chem. Soc. Rev.* **2018**, *47*, 2280–2297; b) J. Zhang, Z. Liu, P. Lian, J. Qian, X. Li, L. Wang, W. Fu, L. Chen, X. Wei, C. Li, *Chem. Sci.* **2016**, *7*, 5995–6005; c) H. S. Jung, J.-H. Lee, K. Kim, S. Koo, P. Verwilst, J. L. Sessler, C. Kang, J. S. Kim, *J. Am. Chem. Soc.* **2017**, *139*, 9972–9978.

[7] a) Y.-J. Gong, X.-B. Zhang, G.-J. Mao, L. Su, H.-M. Meng, W. Tan, S. Feng, G. Zhang, *Chem. Sci.* **2016**, *7*, 2275–2285; b) M. Grzybowski, M. Taki, K. Senda, Y. Sato, T. Ariyoshi, Y. Okada, R. Kawakami, T. Imamura, S. Yamaguchi, *Angew. Chem. Int. Ed.* **2018**, *57*, 10137–10141.

[8] a) A. J. Bard, *Electrogenerated Chemiluminescence*, CRC Press, New York, **2004**; b) M. M. Richter, *Chem. Rev.* **2004**, *104*, 3003–3036; c) W. Miao, *Chem. Rev.* **2008**, *108*, 2506–2553; d) L. Hu, G. Xu, *Chem. Soc. Rev.* **2010**, *39*, 3275–3304; e) Z. Liu, W. Qi, G. Xu, *Chem. Soc. Rev.* **2015**, *44*, 3117–3142.

[9] a) G. Valenti, S. Scarabino, B. Goudeau, A. Lesch, M. Jović, E. Villani, M. Sentic, S. Rapino, S. Arbault, F. Paolucci, N. Sojic, *J. Am. Chem. Soc.* **2017**, *139*, 16830–16837; b) S. Voci, B. Goudeau, G. Valenti, A. Lesch, M. Jović, S. Rapino, F. Paolucci, S. Arbault, N. Sojic, *J. Am. Chem. Soc.* **2018**, *140*, 14753–14760.

[10] a) R. Kurita, K. Arai, K. Nakamoto, D. Kato, O. Niwa, *Anal. Chem.* **2010**, *82*, 1692–1697; b) R. Kurita, K. Arai, K. Nakamoto, D. Kato, O. Niwa, *Anal. Chem.* **2012**, *84*, 1799–1803; c) Y. Chen, J. Xu, J. Su, Y. Xiang, R. Yuan, Y. Chai, *Anal. Chem.* **2012**, *84*, 7750–7755.

[11] a) M. Hesari, Z. Ding, *J. Electrochem. Soc.* **2016**, *163*, H3116–H3131; b) R. J. Forster, P. Bertoncello, T. E. Keyes, *Annu. Rev. Anal. Chem.* **2009**, *2*, 359–385.

[12] a) K. N. Swanick, M. Hesari, M. S. Workentin, Z. Ding, *J. Am. Chem. Soc.* **2012**, *134*, 15205–15208; b) R. Cui, Y.-P. Gu, L. Bao, J.-Y. Zhao, B.-P. Qi, Z.-L. Zhang, Z.-X. Xie, D.-W. Pang, *Anal. Chem.* **2012**, *84*, 8932–8935; c) J. Wang, H. Han, X. Jiang, L. Huang, L. Chen, N. Li, *Anal. Chem.* **2012**, *84*, 4893–4899; d) M. Hesari, M. S. Workentin, Z. Ding, *Chem. Eur. J.* **2014**, *20*, 15116–15121; e) M. Hesari, Z. Ding, M. S. Workentin, *Organometallics* **2014**, *33*, 4888–4892; f) T. Wang, D. Wang, J. W. Padelford, J. Jiang, G. Wang, *J. Am. Chem. Soc.* **2016**, *138*, 6380–6383; g) J. M. Kim, S. Jeong, J. K. Song, J. Kim, *Chem. Commun.* **2018**, *54*, 2838–2841; h) S. Kesarkar, E. Rampazzo, G. Valenti, M. Marcaccio, A. Bossi, L. Prodi, F. Paolucci, *ChemElectroChem* **2017**, *4*, 1690–1696; i) M. Hesari, Z. Ding, *Acc. Chem. Res.* **2017**, *50*, 218–230.

[13] M. Hesari, M. S. Workentin, Z. Ding, *Chem. Sci.* **2014**, *5*, 3814–3822.

[14] M. Hesari, M. S. Workentin, Z. Ding, *ACS Nano* **2014**, *8*, 8543–8553.

[15] X. Long, X. Tan, Y. He, G. Zou, *J. Mater. Chem. C* **2017**, *5*, 12393–12399.

[16] a) S. K. Lee, M. M. Richter, L. Strekowski, A. J. Bard, *Anal. Chem.* **1997**, *69*, 4126–4133; b) S. K. Lee, A. J. Bard, *Anal. Lett.* **1998**, *31*, 2209–2229.

[17] J. Fabian, H. Nakazumi, M. Matsuoka, *Chem. Rev.* **1992**, *92*, 1197–1226.

[18] R. R. Maar, S. M. Barbon, N. Sharma, H. Groom, L. G. Luyt, J. B. Gilroy, *Chem. Eur. J.* **2015**, *21*, 15589–15599.

[19] S. M. Barbon, P. A. Reinkeluers, J. T. Price, V. N. Staroverov, J. B. Gilroy, *Chem. Eur. J.* **2014**, *20*, 11340–11344.

[20] J. R. Rumble, *CRC Handbook of Chemistry and Physics,* 98th ed., CRC Press/Taylor and Francis, Boca Raton, FL.

[21] a) M.-C. Chang, E. Otten, *Chem. Commun.* **2014**, *50*, 7431–7433; b) M.-C. Chang, A. Chantzis, D. Jacquemin, E. Otten, *Dalton Trans.* **2016**, *45*, 9477–9484.

[22] S. M. Barbon, V. N. Staroverov, J. B. Gilroy, *J. Org. Chem.* **2015**, *80*, 5226–5235.
[23] R. Englman, J. Jortner, *Mol. Phys.* **1970**, *18*, 145–164.
[24] R. Y. Lai, A. J. Bard, *J. Phys. Chem. A* **2003**, *107*, 3335–3340.
[25] a) M. Hesari, S. M. Barbon, V. N. Staroverov, Z. Ding, J. B. Gilroy, *Chem. Commun.* **2015**, *51*, 3766–3769; b) M. Hesari, S. M. Barbon, R. B. Mendes, V. N. Staroverov, Z. Ding, J. B. Gilroy, *J. Phys. Chem. C* **2018**, *122*, 1258–1266.
[26] A. B. Nepomnyashchii, S. Cho, P. J. Rossky, A. J. Bard, *J. Am. Chem. Soc.* **2010**, *132*, 17550–17559.
[27] a) M. Hesari, J.-s. Lu, S. Wang, Z. Ding, *Chem. Commun.* **2015**, *51*, 1081–1084; b) A. B. Nepomnyashchii, M. Bröring, J. Ahrens, R. Krüger, A. J. Bard, *J. Phys. Chem. C* **2010**, *114*, 14453–14460.
[28] R. R. Maar, J. B. Gilroy, *J. Mater. Chem. C* **2016**, *4*, 6478–6482.

Layout 2:

COMMUNICATION

Two-step synthesis ***Near-infrared PL & ECL***

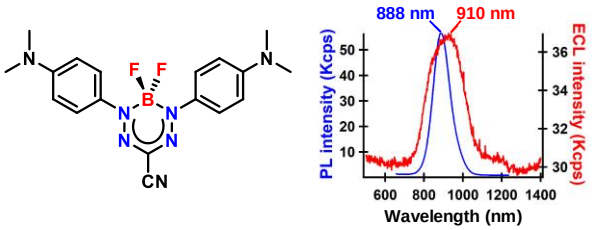

An exceptionally simple boron difluoride formazanate dye, produced in two straightforward synthetic steps, exhibits near-infrared photoluminescence and electrochemiluminescence.

Ryan R. Maar†, Ruizhong Zhang†, David G. Stephens, Zhifeng Ding and Joe B. Gilroy**

Page No. – Page No.

Near-Infrared Photoluminescence and Electrochemiluminescence from an Exceptionally Simple Boron Difluoride Formazanate Dye